An investigation on titanium doping in reduced graphene oxide by RF magnetron sputtering for dye-sensitized solar cells

Foo Wah Low[a,b,*], Chin Wei Lai[b], Nilofar Asim[d], Md. Akhtaruzzaman[d], Mohammad Alghoul[e], Sieh Kiong Tiong[a], Nowshad Amin[a,c,*]

[a] Institute of Sustainable Energy, Universiti Tenaga Nasional (@The National Energy University), Jalan IKRAM-UNITEN, 43000 Kajang Selangor, Malaysia
[b] Nanotechnology & Catalysis Research Centre (NANOCAT), Level 3, IAS Building, University of Malaya (UM), 50603 Kuala Lumpur, MALAYSIA
[c] INTEGRA, Faculty of Engineering and Built Environment, The National University of Malaysia, 43600 Bangi, Selangor, Malaysia
[d] Solar Energy Research Institute, The National University of Malaysia, Malaysia
[e] Center of Research Excellence in Renewable Energy, King Fahd University of Petroleum & Minerals, Dhahran 31261, Saudi Arabia

ARTICLE INFO

ABSTRACT

A study investigating the effects of titanium (Ti) atoms sputtered from different sources on substrate distance was attempted in order to effectively dope a reduced graphene oxide (rGO) thin film surface. Factors such as crystallinity, morphology, phase formation, light absorption, and surface chemical state of rGO-TiO$_2$ were investigated. As a result, functional groups or chemical states revealed the presence of Ti-O-C in rGO-TiO$_2$ nanocomposite after the sputtering process. The titanium source from the target was of Ti^{3+} species as determined using X-ray photoelectron spectroscopy (XPS). It was found that average sized Ti^{3+} ions of around 59.4 nm were incorporated into the rGO nanosheet. A customized Dye-Sensitized Solar Cells (DSSCs) device was fabricated with the photo-anode consisting of sputtered rGO-TiO$_2$ nanocomposite. After optimization, the Ti target allocated with 10 cm-apart FTO glass-coated rGO nanosheet and 0.67 cm^2 active area exhibited an ideal PCE of 6.60%, which is remarkably higher than the usual 5 cm sputtering distance the sample (1.90%) had achieved.

1. Introduction

Aligned to the rapid industrialization, techno-economic growth as well as population increase factors, fossil fuel based energy demand is estimated to double in growth by the year 2050 (Berardi, 2017). Conventional energy sources like oil, natural gas, and coals have been proven to cause global warming, air pollution from CO$_2$ gas emissions, and erratic weather patterns. Hence, researchers have explored alternative green energy sources to replace of the traditional fossil fuels. Carbon-free renewable energy such as hydropower, biomass, wind, geothermal, ocean energy, nuclear fission, and solar are alternate sources of energy that provide a solution to overcome the environment pollution issue in a sustainable manner (Chandra and Gill, 2017).

Sunlight is the most abundant, reliable, and clean energy source available which could be converted into useful electricity. Thus, solar energy is the most promising source as 0.1% received conversion from sunlight through photovoltaic cell could produce up to 10% of power conversion efficiency (PCE) performance (Shang et al., 2015). However, the efficiency and production cost of solar cells is one of the shortcomings of this sustainable technology. Although there are drawbacks, the third generation of the photovoltaic cell, Dye-Sensitized Solar Cells (DSSCs) are an auspicious technology due to their ease of fabrication, cost effectiveness, and reasonable PCE performance (Hagfeldt and Vlachpoulos, 2018; Giordano et al., 2016). Basically, a DSSCS is composed of four main interfaces: FTO/photo-anode, Photocatalyst/dye, dye/electrolyte, and electrolyte/counter electrode. In the past two decades, a lot of researchers have focused on FTO/photo-anode interfaces in order to obtain a unidirectional charge flow with no electron leakage. In this interface, carbon-based material has attracted cosmic interest as a photoelectrode used to fasten the electron flow from dye into the FTO glass in the photo-anode site (Kim et al., 2009). Graphene or Reduced Graphene Oxide (rGO) was found to be the best candidate to reduce back-transport reactions in DSSCs (Kazmi et al., 2017). Graphene is a monolayer of sp^2-bonded carbon atoms arranged in a honeycomb structure as a two-dimensional material (Gómez-Navarro et al., 2010). Since its discovery in 2004, it has attracted numerous attention

due to its astonishing electrical, chemical, mechanical, and thermal properties (Achee et al., 2018; Wei et al., 2018; Al-Rawashdeh et al., 2018; Novoselov et al., 2004). The two dimensional π-π conjugation structure of graphene has the ability to provide excellent conductivity as an electron charge carrier transport in DSSCs (Xiang et al., 2011). However, graphene itself can only absorb 2.3% of visible light over the vis-NIR range (Yu et al., 2016).

In order to enhance its photo-absorption activity, metal oxide is incorporated into graphene photoelectrodes as an obligatory step for photocatalytic activity purposes. Among the various metal oxides, Titanium Dioxide (TiO$_2$) is most widely used in DSSCs due to its long-term thermodynamic stability, excellent photochemical stability, low cost, and relative toxicity (Fujishima et al., 2008). However, TiO$_2$ itself exhibits a recombination of electrons and holes and also a wide band gap of anatase TiO$_2$ with 3.2 eV, resulting in a low photocatalytic level for DSSCs' applications (Tan et al., 2013). Additionally, the TiO$_2$ layer may cause an electrical short at the electrolyte/counter electrode interface (Jin et al., 2012). Therefore, some researchers have experimented on the preparation of graphene-TiO$_2$ or rGO-TiO$_2$ hybrid as photo-anode in DSSCs (Lim et al., 2015; Ding et al., 2015; Song et al., 2011). This hybridization could improve the movement of excited electrons from dye into the CB of TiO$_2$ where rGO acts as electron facilitator into FTO. The heterojunction formed by rGO-TiO$_2$ (Schottky barrier) enables the separation of photoinduced electron-hole pairs and suppressed charge recombination (Xiang et al., 2011).

In 2010, Williams and his co-researchers pioneered the modification of graphene-based metal oxide composites for the purpose of enhancing its photocatalytic activity (Williams et al., 2008). To date, Zhang et al. (2017), Tang and Hu (2012), and Nouri et al. (2016) have fabricated hydrothermal methods to prepare rGO-TiO$_2$ composite materials and showed that these composites exhibit enhanced photoactivity towards PCE of DSSCs. On the other hand, Guo et al. conducted a research on rGO-TiO$_2$ composites prepared by molecular grafting technique with Ti (OBu)$_4$ source. However, these preparation methods had not achieved the desired level of DSSCs performance. The main reason is that the TiO$_2$ molecules were not deposited well on the rGO to form Ti-O-C bonds. Therefore, the magnetron sputtering method is one of the promising potential approaches to further improve the contact interfaces between graphene basal plane and TiO$_2$. Using this technique, the TiO$_2$ target could also offer an efficient Ti^{3+} ion sputter on rGO nanosheet at a uniform thickness. In addition, it could also produce composites at a large scale, provide ease of control, as well as is low-cost in production. Table 1 tabulates the PCE performance of sputtered Ti ions with graphene/GO as photo-anode element in DSSCs. However, the crystal quality of Fluorine-based of FTO is reduced due to the high energy induced ions bombardment during the sputtering process (Jäger et al., 2014). Up to date, there are still only a few researches on the formation of TiO$_2$ using graphene/rGO via the sputtering method for the purpose of enhancing DSSCS performance. However, it is indeed proven that rGO-TiO$_2$ nanocomposites can be of great use in DSSCs.

In this paper, we present a RF magnetron sputtering method for the preparation of rGO-TiO$_2$ nanocomposites as photo-anodes for DSSCs devices. An optimized Ti target to rGO nanosheet sample distance in the sputtering process could minimize the loss of electrons upon suppression of the recombination centre, hence maximizing the photo-induced charge carrier transport as well as PCE performance of DSSCs. Here, we

report that the RF magnetron sputtering is a better technique compared to conventional synthesis due to its highly accelerated Ti^{3+} species sputtered neither on the rGO surface nor into the lattice within a shorter time (Low et al., 2017). In fact, this technique relies on the ion bombardment of energetic Ti^{3+} ions to provide a better adhesion of TiO$_2$ dopants on rGO nanosheets. So far, studies on the incorporation of TiO$_2$ into rGO nanosheets at various sputtering distances from the Ti target to the rGO substrate for application in DSSCs are still lacking. The effect of various distances used to sputter Ti^{3+} species onto ultrathin rGO to produce efficient photo-anodes for DSSCs remains unclear. Therefore, comprehensive works were carried out to optimize the sputtering distance in order to obtain an ideal rGO-TiO$_2$ nanocomposite film under 100 W of solar illumination.

2. Experimental details

2.1. Material preparation

Graphite flakes (< 45 μm; ≥ 99.99%), postassium permanganate (KMnO$_4$; 97%), hydrazine (35 wt% solution in water), triton X-100, fluorine doped tin oxide coated glass slide (FTO) with surface resistivity of ~7 Ω/sq, and Di-tetrabutylammonium *cis*-bis(isothiocyanato)bis (2,2′-bipyridyl-4,4′-dicarboxylato)ruthenium(II) (N-719) dye were purchased from Sigma-Aldrich, Malaysia. Sulfuric acid (H$_2$SO$_4$; 0.5 M), phosphoric acid (H$_3$PO$_4$; 85%), and hydrogen peroxide (H$_2$O$_2$; 30%) were purchased from Chemolab, Malaysia. Hydrochloric acid (HCl; 37%), acetonitrile (C$_2$H$_3$N; 41.05 g/mol), absolute ethanol (≥99.5%), and potassium iodide (KI; ≥99.0%) electrolyte were purchased from Merck, Malaysia.

2.2. GO and rGO nanosheet preparation

From our previous work, GO and rGO nanosheets were obtained via an optimized Improved Hummer's Method and Chemical Reduction Method, respectively (Low et al., 2015a, 2015b). Using typical procedures, GO was synthesized form graphite flakes via the Improved Hummer's method. A mixture of graphite (1.5 g) and KMnO$_4$ (9.0 g) was added into an acid ratio of 9:1 (H$_2$SO$_4$:H$_3$PO$_4$) solution. The solution was stirred under ice-water bath conditions (< 20 °C) for 24 h (Marcano et al., 2010). After 24 h, the color of mixture noticeably changed from dark purplish green to dark brown. The mixture was then poured into an ice container (≈ 200 mL) and 3 mL of H$_2$O$_2$ was dropped slowly into the mixture to terminate its oxidation process. The mixture changed color immediately to light brownish after the addition of H$_2$O$_2$, indicating a high oxidation level of graphite (Marcano et al., 2010). The mixture was then centrifuged and the supernatant was decanted away. The remaining solid material was washed with HCl and deionized (DI) water. Finalize, GO was formed after the material was dried overnight using a drying oven. For the rGO synthesis, GO powder was added into 3 mg/mL distilled water. After that, hydrazine solvent was then added immediately along with 1 μL/3 mg of GO into the mixture. The mixture was then heated at 80 °C under oil bath conditions to stabilize the mixture (Park et al., 2011). The mixture was centrifuged for 1 h, and unwanted residue was removed. The finalized rGO product was obtained after the material was dried in a drying oven at 90 °C for 48 h.

Table 1
List of sputtering techniques based rGO-TiO$_2$ nanocomposite for DSSCs.

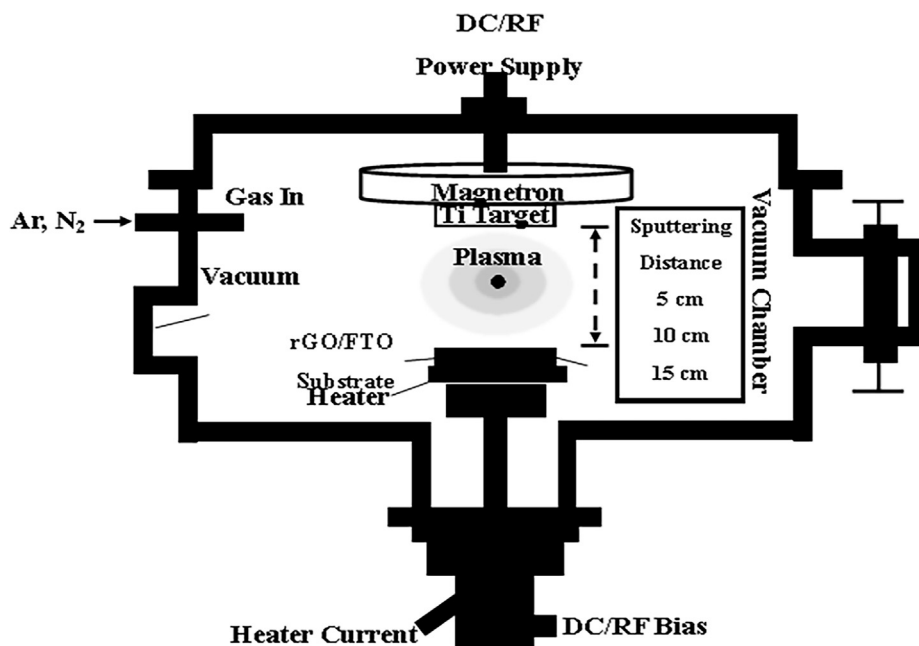| Amount of graphene	Short circuit current density, Jsc, mA/cm^2	Open circuit voltage, Voc	Fill factor, ff	PCE, η (%)	Ref./Year
N/A	11.2	0.68	0.49	3.80	(Jäger, 2014)/2009
N/A	17.5	0.50	0.46	3.98	(Low et al., 2017)/2015
N/A	7.60	0.67	0.54	2.78	(Low et al., 2015)/2016
GO:TiO$_2$ (0.005:1)	5.11	0.78	0.64	2.56	(Low et al., 2015)/2017
1.3 wt%	5.15	0.58	0.60	1.81	(Marcano, 2010)/2017

Fig. 1. Illustration of rGO-TiO$_2$ nanocomposite formation in RF Magnetron sputtering.

2.3. rGO deposition and rGO-TiO$_2$ nanocoposite formation

The rGO-TiO$_2$ nanocomposite was prepared as efficient photo-anodes for the use in DSSCS devices. Prior to that, the rGO nanosheet was deposited as a first layer on the FTO glass using the 2 cm × 2 cm electrodeposition method reported earlier (Low et al., 2015). The active area of rGO deposition was fixed at 0.67 cm^2 for both electrodes (anode and cathode). The researchers also reported the formation of a hybrid rGO-TiO$_2$ nanocomposite via the sputtering process for the purpose of testing its implantation power and variation in sputtering duration parameter on DSSCS performance (Low et al., 2017, 2018). In this typical procedure, a FTO glass containing a rGO nanosheet was sputtered using the RF magnetron sputtering process with Ti^{3+} ions to obtain a rGO-TiO$_2$ nanocomposite at a variation of sputtering distances of 5 cm, 10 cm, 15 cm, 20 cm, and 25 cm apart. The complete schematic diagram for the RF sputtering process is shown in Fig. 1. A titanium target (99.99% purity, diameter in 50,800 μm and thickness in 6350 μm) was used in the sputtering process. The reason for utilizing the RF sputtering technique instead of the conventional method is the ability to generate high acceleration of Ti^{3+} ions onto the rGO surface which penetrates into the rGO lattice in the flash period (Yen et al., 2011). In this situation, the sputtering process enhances the electron transport rate, resulting in high PCE performance. The sputtering duration and input power were fixed at 60 s and 150 W under Ar gas flow rate at 15 mL/min to assure that the Ti^{3+} ions were deposited uniformly onto the rGO nanosheet. Furthermore, the sputter process was set at a constant of 266.64 mPa and a base pressure of 0.67 mPa. A FTO glass deposited with rGO-TiO$_2$ nanocomposite was formed as photo-anode for further DSSCS fabrication.

2.4. DSSC fabrication

Fig. 2 illustrates the chemical structure of the rGO-TiO$_2$ nanocomposite as photo-anode section and a schematic diagram of a working DSSCS. Basically, a DSSCS device has a sandwich configuration consisting of FTO glass, photo-anode for visible light absorption, cathode, N-719 dye, and KI electrolyte. For the construction, a photo-anode based rGO-TiO$_2$ was soaked in a solvent containing 0.5 Mm N-719 dye and absolute ethanol overnight. Next, the photo-anode was rinsed with acetonitrile and dried out for 10 mins on a hot plate. After

that, both electrodes were sandwiched together and clipped with a paper clip. Lastly, 0.5 M KI electrolytes were dropped between electrodes.

2.5. Characterization

The phase of the synthesized hybrid rGO-TiO$_2$ nanocomposites was characterized through X-ray diffraction (XRD) using a D8 Advance X-ray diffractometer-Bruker AXS with a scanning rate of 0.033 deg/s in 20° to 70° with Cu Kα radiation (λ = 0.15418 nm) operated at 40 kV and 30 mA. The surface morphologies were viewed using field emission scanning electron microscope (FESEM, FEI Quanta 200 FEG), high-resolution transmission electron microscopy (HRTEM) using a JEM 2100F with 200 kV accelerating voltage, Tecnai G2 transmission electron microscope (TEM). The elemental analysis of the rGO-TiO$_2$ nanocomposite was determined using energy dispersion X-ray (EDX microanalysis) under 5 kV equipped in the FESEM. The chemical states of the rGO-TiO$_2$ nanocomposite were analyzed using photoelectron spectroscopy (XPS, PHI Quantera II instrument) with a dual X-ray source. Overall binding energies were calibrated using contaminant carbon (C 1s, 284.6 eV) as benchmark. Raman analysis was performed using Renishaw inVia microscope (HeCd laser source, λ = 514.0 nm) for structural identification purposes. Functional groups of GO, rGO, anatase TiO$_2$, and rGO-TiO$_2$ nanocomposite were identified through attenuated total reflection Fourier-transform infrared (ATR-FTIR) spectroscopy. The ATR-FTIR was performed using a FTIR-spectrum 400 instrument, Perkin Almer at the range of 500 to 4000 cm^{-1}. The optical properties of rGO-TiO$_2$ under a variation of sputtering distances were determined using a UV–visible-diffuse reflectance spectrophotometer (UV-2600, Shimadzu Co.). The overall performance of the DSSCs were recorded using a Autolab potentiostat, PGSTAT204 instrument under solar irradiation with an input power of 100 W (Mercury Xenon Lamp-based Newport 66902 instrument) and elaborated into *J-V* curves.

3. Results and discussion

XRD pattern was utilized to investigate the presence and influence of the introduced materials on the crystallinity of rGO nanosheets. Fig. 3 shows the XRD patterns for synthesized rGO, anatase TiO$_2$, and distance of Ti^{3+} ions sputter source on rGO nanosheet which formed
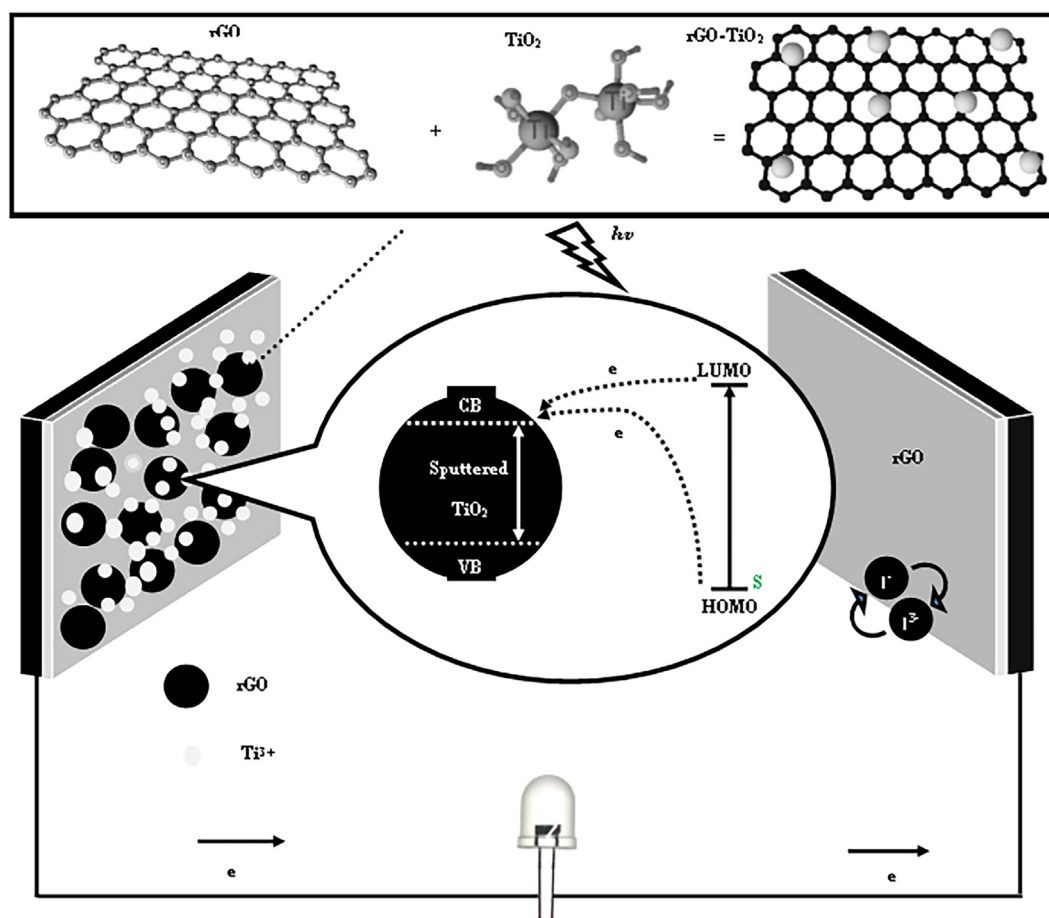
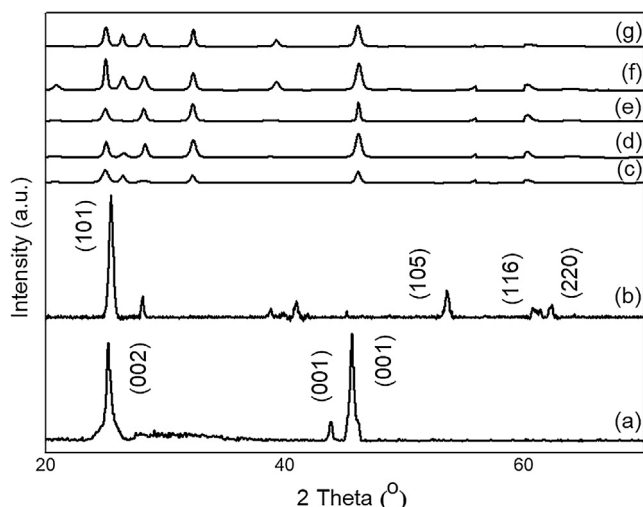Fig. 2. Schematic of rGO-TiO$_2$ nanocomposite photoanode in DSSCs.

Fig. 3. XRD patterns of (a) as-prepared rGO, (b) Anatase TiO$_2$, and Sputtered Ti^{3+} on rGO nanosheet at distances of (c) 5 cm, (d) 10 cm, (e) 15 cm, (f) 20 cm, and (g) 25 cm.

the rGO-TiO$_2$ nanocomposite. In the authors' previous work, they have demonstrated that the peak orientation for rGO nanosheet (refer Fig. 3a) and anatase TiO$_2$ is in good agreement with JCPDS 21-1272 (refer Fig. 3b) (Low et al., 2018, 2017). The XRD patterns in (c) to (g) were well aligned with the major peaks of rGO at 25.3°, 43.8°, and 45.6° with acknowledgement along the (0 0 2) and (0 0 1) orientations and also the anatase TiO$_2$ crystallinity phase at 25.4° along the (1 0 1)

orientation. In addition, the appearance of intensive peaks at 25° and 26.5° corresponded to the d spacing of 0.36 nm and represented a full reduction of GO to graphene where it was also sputtered with Ti^{3+} except for the 15 cm sample along 25° (Štengl et al., 2013).

The morphologies of GO and rGO were viewed under FESEM imaging. Fig. 4a shows an uneven multilayer of graphite stacked up to form GO with very thin layers. However, some of layers obtained were much thinner that they looked akin to rGO layers. Similar morphological features were observed for the rGO nanosheet. It was obtained as a single layer after reduction (refer Fig. 4b). In the authors' previous work, they managed to synthesize the rGO in ultrathin layers at nanoscale (around 47 nm) with good conductivity results (Low et al., 2015). Subsequently, the morphology of the rGO-TiO$_2$ nanocomposite was further observed using a TEM instrument as shown in Fig. 4c. As aforementioned, Ti^{3+} ions of TiO$_2$ were sputtered onto rGO nanosheets to form a rGO-TiO$_2$ nanocomposite. The dark color represents the rGO nanosheet whereas the white color with a rice-like shape represents TiO$_2$ nanoparticles. The average TiO$_2$ nanoparticle size obtained was around 59.4 nm. The blue circled inset in Fig. 4c identified the related composition under the EDX analysis tool (10 cm sputtered sample). Details of the corresponding elements in rGO-TiO$_2$ are listed in Table 2. For the experiment using 5 cm sputter distance of Ti^{3+} ions, the Ti element contents achieved the highest ratio at 53.56%. This is the highest amount of Ti^{3+} ions reacting with the rGO nanosheet, resulting in the increased or charged recombination rate of the electrolyte and also resistance of hole-pairs separation (Rambabu et al., 2016). In other words, closer sputter distance result in TiO$_2$ bulk formation onto the rGO nanosheets which thus reduces the hole transfer rate towards the electrolyte at the rGO-TiO$_2$/electrolyte interface. Besides, the Ti element composition proved that the longer the sputter distance; the lesser
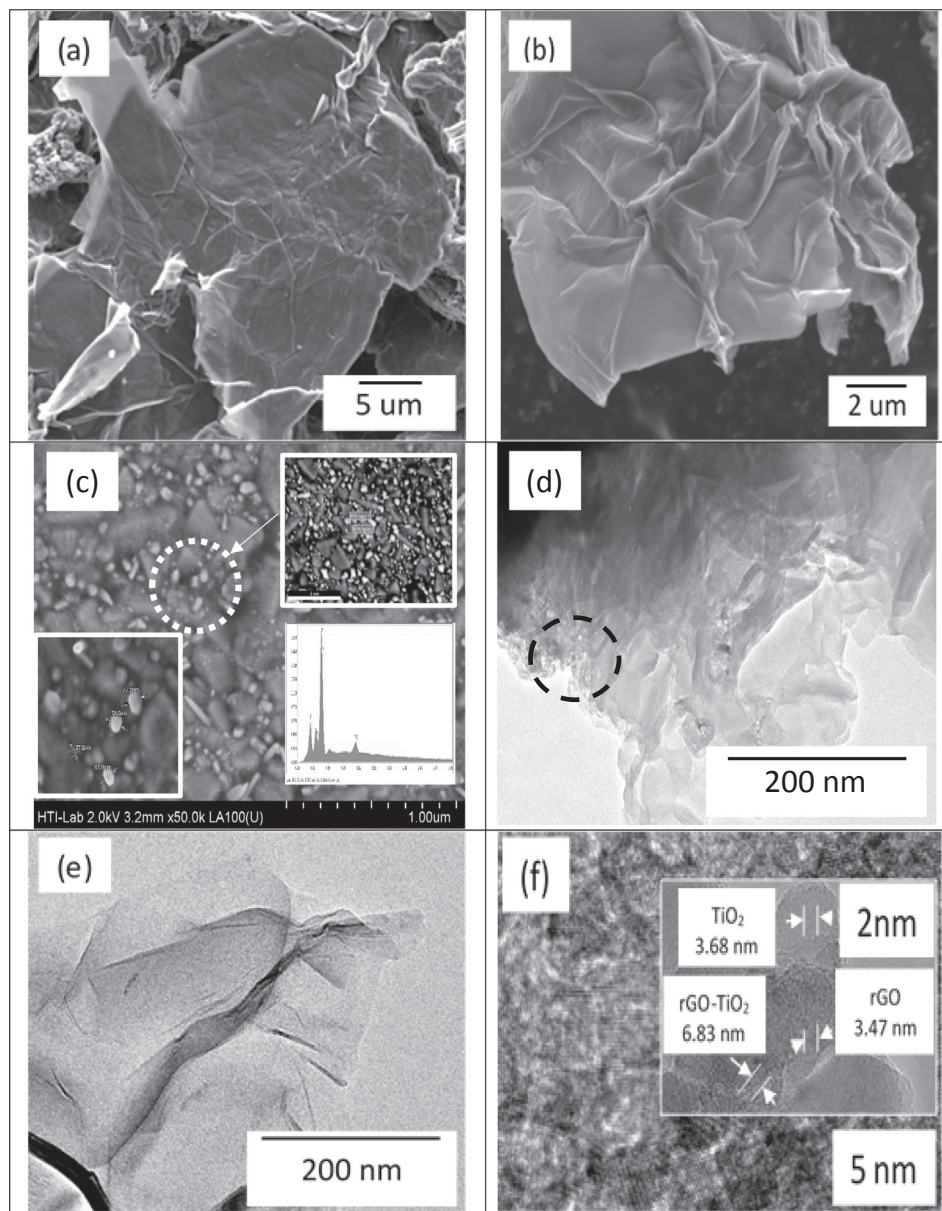
Fig. 4. FESEM images of (a) GO, (b) rGO, (c) rGO-TiO$_2$; HRTEM images of (d) GO and (e) rGO; TEM image of (f) rGO-TiO$_2$ nanocomposite.

Table 2
EDX analysis of rGO-TiO$_2$ nanocomposites based sputtered distance.

Sputtering distance (cm)	Atomic, at (%)			
	Carbon, C	Titanium, Ti	Oxygen, O	Magnesium, Mg
5	11.98	53.56	32.02	2.44
10	23.54	28.19	45.84	2.43
15	23.33	28.14	46.24	2.29
20	21.93	27.47	48.23	2.37
25	23.92	23.77	50.01	2.30

the amount of Ti. Besides, the O element's composition increased dramatically due to the contribution of rGO and double bond of TiO$_2$. Moreover, the C element also increased with the longer sputter distance, revealing lesser sputtered amount of Ti^{3+} ions onto the rGO nanosheet. Lastly, a less intense Mg element was also present mainly from the mixer substance during the sputtering process.

HRTEM was utilized for further inspection of the GO and rGO structure. In Fig. 4d, the GO was formed as an agglomeration with unequal layers. The darker color area at the left upper denote the multilayers of GO formed, whereas the brighter color at the middle bottom area prove the existence of lesser stacks of GO layers. Moreover, the existence of white dots along the GO layer (circled) signifies the strong bonding between oxygenated molecules and carbon basal planes. The oxidation process successfully modified the graphite material to form the GO product (Thakur and Karak, 2012). The rGO product was also observed using HRTEM imaging. The image clearly demonstrated that the rGO is a silk-like structured monolayer as shown in Fig. 4e. However, there are also some staking or folding layers of graphene as denoted by the dark color. Lastly, further exposure of the lattice of the rGO-TiO$_2$ nanocomposite was conducted using TEM imaging (Fig. 4f). The rGO-TiO$_2$ nanocomposite was shown to have three intermediate colors; the darker color symbolizes the sputtered TiO$_2$, the brighter color is the rGO layer, and the other layer represents the rGO-TiO$_2$ nanocomposite. The lattice measurements of rGO, TiO$_2$, and rGO-TiO$_2$ nanocomposite as insets are 3.47 nm, 3.68 nm, and 6.83 nm, respectively, and all together are comprised of 10 layers. Hence, the interlayer distances of rGO, TiO$_2$, and rGO-TiO$_2$ were 0.35 nm, 0.37 nm, and
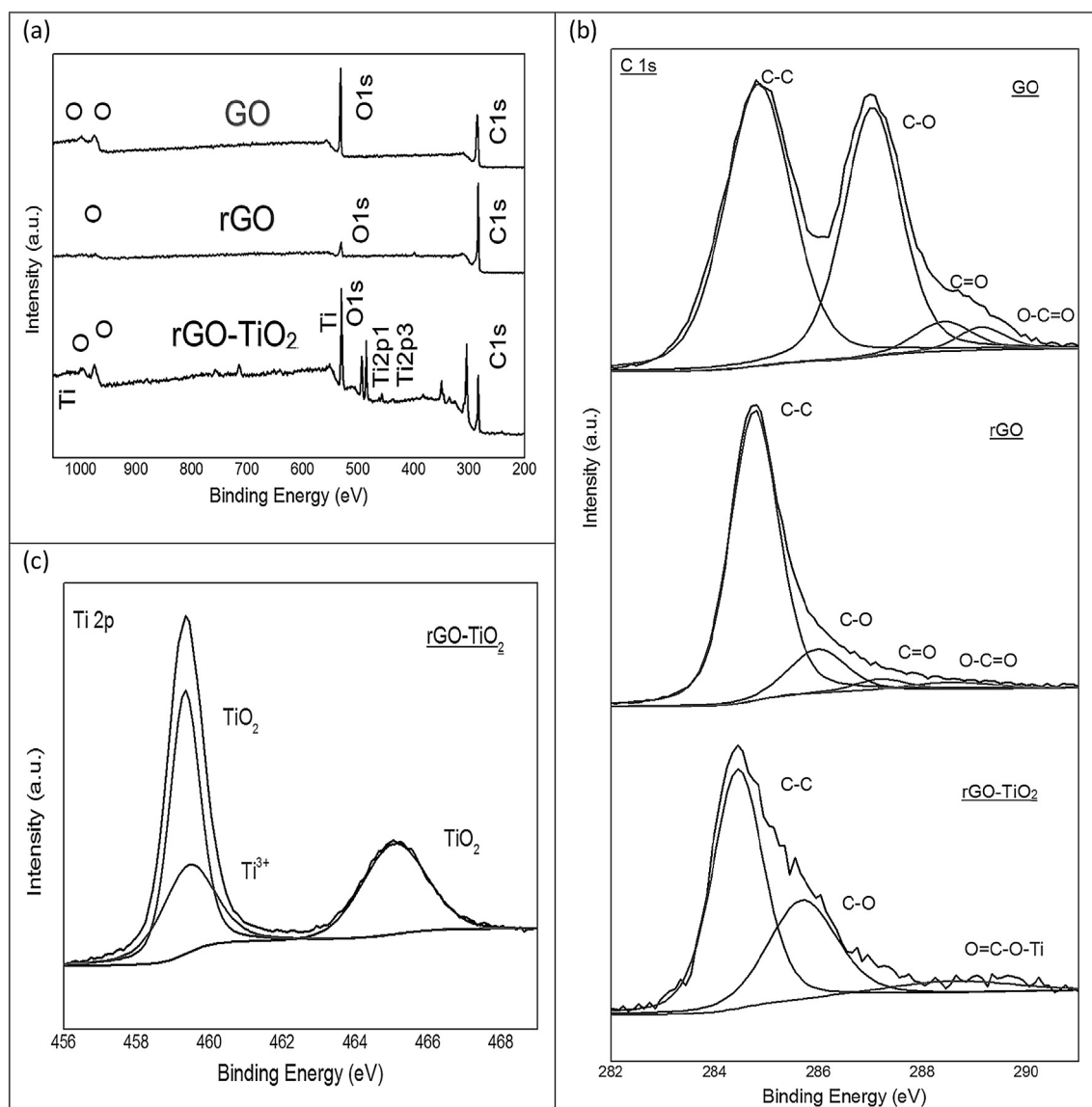
Fig. 5. XPS spectra of (a) survey patterns of GO, rGO, and rGO-TiO₂, (b) C1s of GO, rGO, and rGO-TiO₂, and (c) Ti 2p of rGO-TiO₂.

0.68 nm, respectively. These results are in agreement with the XRD results.

The surface chemical state was analyzed using the XPS instrument. Fig. 5 shows the spectra based on the chemical elements of the GO, rGO, and rGO-TiO₂ nanocomposite accordingly. As shown by the spectra, the synthesis of GO and rGO nanosheet mainly contributed the C 1s and O 1s element. Fig. 5a clearly shows a great decrease of O1s (~530.0 eV) and disappearance of O (around 960.0–970.0 eV), indicating deoxygenation in the GO to form the rGO. In contrast, the C 1s (around 290.0 eV) of rGO had gradually increased compared to that in the GO. The reduction of oxide functional groups, O in the rGO nanosheet strengthened the Carbon bonding (Low et al., 2015). Besides, the survey spectrum of the rGO-TiO₂ nanocomposite contributed to the Carbon, Oxygen, and Titanium species. The presence of Ti, Ti 2p1, and Ti 2p3 in this composite is in good agreement with its good bonding with the rGO nanosheet. Moreover, the increase of O element showed that TiO₂ was well established with the rGO nanosheet, whereas the C element was slightly decreased. The chemical state of C 1s is vital to determine or monitor the actual bonding structure of the GO, rGO, and rGO-TiO₂ nanocomposite (Fig. 5b). C 1s state peaks for these three materials appeared at ~282.0–291.0 eV. The deconvolution of the C 1s of GO attributed to four intense peaks corresponded to the C–C (284.8 eV),

C–O (287.0 eV), C=O (288.4 eV), and O–C=O (289.1 eV) (Lee et al., 2012; Pei et al., 2010). Hereby, rGO was formed from GO since every oxygenated bond had significantly decreased (deoxygenated molecules reaction) during the reduction process by their hydrazine solvent (Yan et al., 2014). Besides, the C–C bond of rGO had significantly increased, indicating that the sp² hybridized carbon network was well-formed after the reduction process of GO. After the rGO nanosheet had incorporated the TiO₂, the degree of oxidation of C–O increased dramatically with the increases in oxygenated functional group. Additionally, the appearance of a O=C–O–Ti peak at the binding energy of 288.6 eV revealed that the Ti–O–C bonding was formed during the sputtering process (Liu, 2014). Furthermore, Fig. 5c shows that the Ti 2p of rGO-TiO₂ intense peaks at 459.3 eV associated with Ti 2p$_{3/2}$ and Ti 2p$_{1/2}$ were observed for the TiO₂ spectrum. Another supporting TiO₂ peak also appeared at 465.1 eV and governed the previous statement. Lastly, it was also proven that the Ti ion source was Ti³⁺ species according to the peak shown at 459.4 eV for the sputtering process.

Raman spectroscopy was used for rGO-TiO₂ composite observation based on their molecular morphology structure and characterization of carbonaceous films. Fig. 6 shows the Raman spectra of rGO, anatase TiO₂, and rGO-TiO₂ nanocomposite. For rGO, two intensive bands were detected at 1350.9 cm⁻¹ (D band) and 1604.9 cm⁻¹ (G band) and were
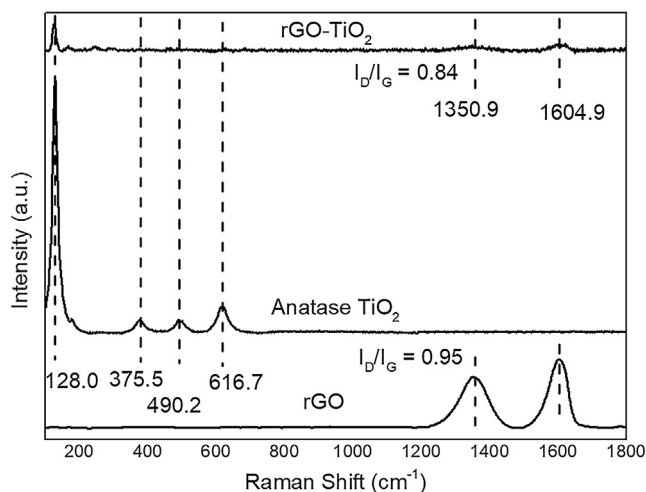
Fig. 6. Raman spectra of rGO, Anatase TiO$_2$, and rGO-TiO$_2$ nanocomposite.

associated with the presence of carbon materials (How et al., 2014). The D band of rGO is due to the sp^3 defects (Gao et al., 2010), whereas the G band is mostly attributed to E$_{2g}$ symmetry of doubly-degenerated phonon mode at the Brillouin zone centre and corresponds to the hexagonal network of sp^2 carbon atoms (Naumenko et al., 2012). Furthermore, a decreased value of I$_D$/I$_G$ ratio of rGO (0.95) to the rGO-TiO$_2$ nanocomposite (0.84) is mainly attributed to the changes from sp^3 to sp^2 hybridized carbon, and also the reduction of sp^2 domain size of carbon atoms during the sputtering process (Zhang et al., 2011; Gao et al., 2011). Besides, some relevant peaks in TiO$_2$ source at 128.0 cm^{-1}, 375.5 cm^{-1}, 490.2 cm^{-1}, and 616.7 cm^{-1} are assigned to the E$_g$, B$_{1g}$, A$_{1g}$, and Eg, respectively. These significant peaks determined that the sputtered ions' source was the anatase phase of TiO$_2$ (Chu et al., 2015). However, the Raman spectra for anatase TiO$_2$ did not appear much in the rGO-TiO$_2$ nanocomposite due to the low amount of Ti ions sputtered onto the rGO nanosheet.

A FTIR analysis was employed to identify the functional groups containing carbon and titanium materials. In Fig. 7a, the FTIR spectra of graphite show no significant functional groups along the orientation. For the GO spectra, the FTIR analysis found an essential broad peak at 3400 cm^{-1} representing the –OH stretching (Wang et al., 2012a). This occurrence revealed that a huge amount of oxygen-containing functional groups was formed during the oxidation process (Fig. 7b). Two small peaks at 2842 cm^{-1} and 2906 cm^{-1} were assigned as CH$_2$
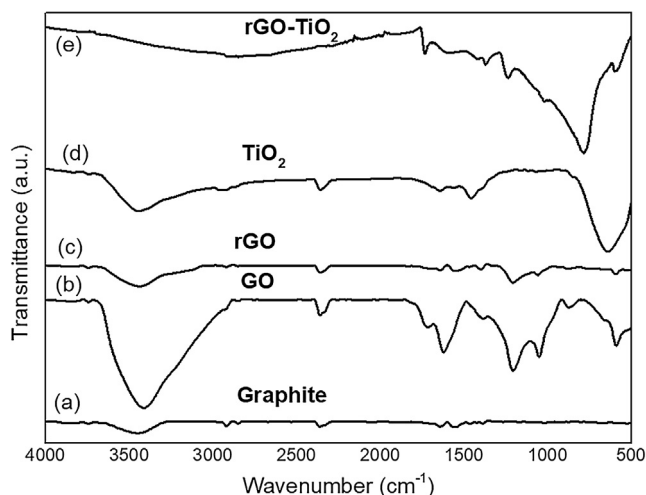

Fig. 7. FTIR spectra of (a) graphite powder, (b) GO, (c) rGO, (d) Anatase TiO$_2$, (e) rGO-TiO$_2$ nanocomposite.

stretching groups (Sher Shah et al., 2012). Moreover, some intense absorption peaks at 862 cm^{-1}, 1054 cm^{-1}, 1218 cm^{-1}, 1623 cm^{-1}, 1735 cm^{-1} were mainly attributed to the aromatic C-H deformation (Wang et al., 2012b), C–O stretching (Zhou et al., 2011), phenolic C–OH stretching (Wang et al., 2012b), –OH (Pan et al., 2012), and C= O stretching (Shen et al., 2011), respectively. In Fig. 7c, all of the absorption bands were dramatically reduced, including –OH group at 3400 cm^{-1} due to the formation of deoxygenated molecules during the reduction process. Besides, Fig. 7d shows the FTIR spectra of anatase TiO$_2$ with three significant peaks at 580 cm^{-1}, 1650 cm^{-1}, and 3400 cm^{-1} assigned as Ti-O-Ti vibration bonds, –OH group, and –OH of the water molecules on the TiO$_2$ surface (Al-Taweel and Saud, 2016). According to Fig. 7e, the FTIR spectra of rGO-TiO$_2$ nanocomposite was found to retain some broad band peaks at 3400 cm^{-1}. These results imply that GO is not fully reduced into graphene to form rGO; this is consistent with the XRD and Raman results. In addition, it can also be considered as residual oxygen-containing vibration band (Tan et al., 2013). In addition, a broad vibration peak at 800 cm^{-1} (Ti-O-Ti stretching modes) addressed to the Ti-O-C bond was formed in the rGO-TiO$_2$ nanocomposite (Jiang et al., 2011). This broad band peak proved that the strong chemical interaction between rGO and TiO$_2$ was formed in agreement with the XPS results. Lastly, the irrelevant band allocated at 1600 cm^{-1} was assigned as the skeletal vibrations of graphitic domains (Li et al., 2015).

A UV–visible (UV–Vis) spectroscopy was used to further explore the optical properties of the semiconductor compound. Fig. 8 demonstrates the comprehensive UV-DRS spectra and Tauc plots for the sputtering distance between the Ti^{3+} ions' source and the rGO nanosheet sample during the sputtering process. It was clearly shown that the range of absorption edges of the rGO-TiO$_2$ nanocomposite from 385 nm (25 cm sample) to 440 nm (10 cm sample) corresponding to the estimated band gap energies, E$_g$ of 2.52 eV and 2.41 eV. The 10 cm distance from the rGO nanosheet implemented shifted towards a higher wavelength compared with the 25 cm sample, suggesting a narrowing band gap due to the introduction of Ti^{3+} ions at a consistent amount and allocated sputter distance. It was found that 10 cm is the precise distance to attract Ti^{3+} ions and facilitate efficient electron transitions from the valence band (VB) to the conduction band (CB), (O$_{2p}$ – Ti$_{3d}$) (Hamid et al., 2014). The optimized band gap of rGO-TiO$_2$ nanocomposite in terms of distance was determined using the Kubelka-Munk (KM) expression for Fig. 8b accordingly by $[F(R)h\nu]^{\frac{1}{2}} = A(h\nu - E_g)$, where

$F(R)$ = KM function;
h = Planck's constant;
ν = Speed of light;
A = Constant;
E_g = Band gap.

The estimated band gaps for rGO-TiO$_2$ nanocomposite were 2.53 eV, 2.41 eV, 2.43 eV, 2.50 eV, and 2.52 eV for 5 cm, 10 cm, 15 cm, 20 cm, and 20 cm, respectively. Among the sputtering distance samples, the 10 cm sample achieved the smallest band gap at $\sim$2.41 eV to produce a reliable introduction of Ti^{3+} ions into rGO nanosheet. However, the 5 cm distance between the Ti^{3+} source and the rGO sample recorded a gap of $\sim$2.53 eV. This small distance suggests that high access of Ti^{3+} ions with rGO weakens the photocatalytic activity and PCE performance.

The current density against voltage characteristic (J-V) curves of DSSCs based on different sputtering distance of Ti^{3+} ions source with the rGO nanosheet are shown in Fig. 9. The photovoltaic parameter details are listed in Table 3. From the table, the J_{sc} value of the 10 cm sample recorded the highest value at 15.82 mA/cm^2, indicating that a consistent introduction of Ti^{3+} ions at the precise sputtering distance could enhance the absorption of photons under visible light conditions. This result is in good agreement with the UV-DRS analysis. Meanwhile, this sample also obtained the highest PCE performance at 6.60%, 3.5
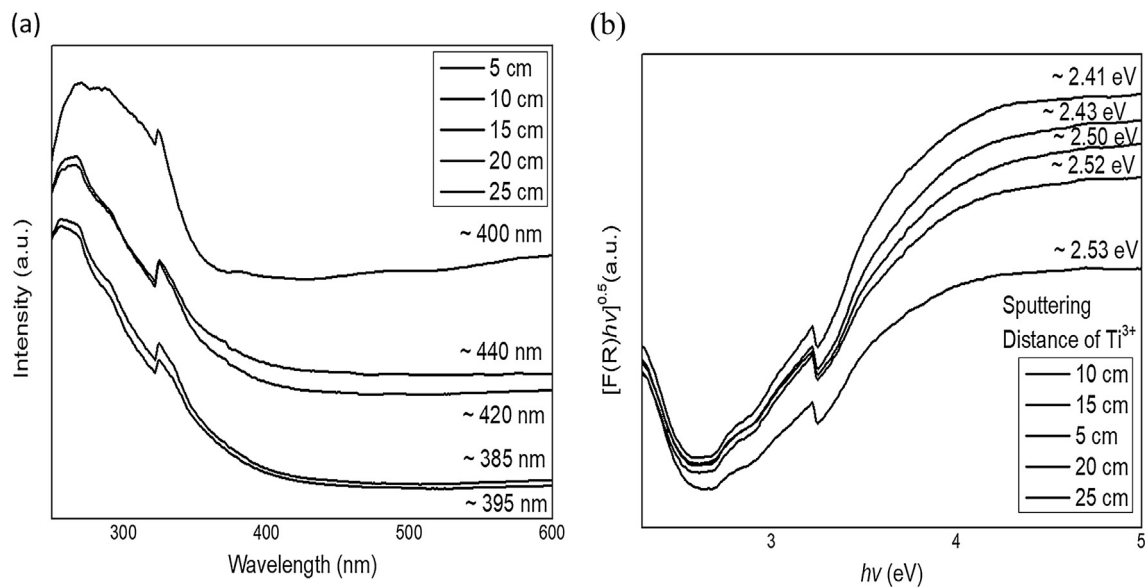
(a)

(b)

Fig. 8. UV–vis reflectance spectra for (a) UV-DRS absorbance and (b) Tauc plots of rGO-TiO$_2$ nanocomposites formed at different sputtering distance.
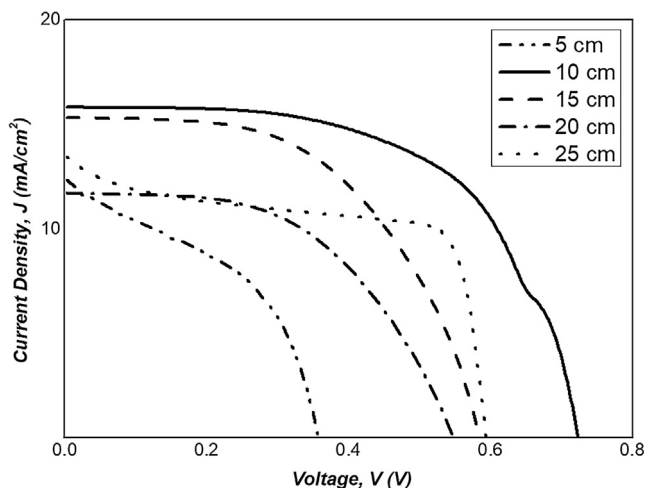

Fig. 9. J-V Curves of the DSSCs with various rGO-TiO$_2$ nanocomposites formed at different sputtering distance.

times higher than that recorded using the 5 cm sputtering distance. The 5 cm sputtering distance only recorded a PCE of 1.91% mainly due to the close sputtering distance which caused a higher level of Ti^{3+} ions reacting onto rGO nanosheet and resulting in an increase in charge recombination rate, photocatalytic activity, and interior resistance (Song et al., 2014). Only 0.68% was achieved using the rGO nanosheet based photo-anode in the authors' previous reported performance due to the poor catalytic light absorption at the photo-anode/FTO interface (Low et al., 2017). In addition, a higher Ti^{3+} loading (5 cm sputtering distance) also increased the charge transport resistance between the dye

and rGO at electrolyte/dye/rGO-TiO$_2$ interface, thus leading to a reduction in the overall PCE performance (Chen et al., 2012).

4. Conclusion

In this study, rGO-TiO$_2$ nanocomposites were successfully fabricated as photo-anodes to improve the PCE of DSSCs. rGO-TiO$_2$ nanocomposites were obtained using different sputtering distances between the Ti^{3+} target and rGO nanosheets via the RF magnetron sputtering technique. The RF magnetron sputtering technique gave the metal Ti^{3+} ions direct penetration into the rGO nanosheet. It was found that the 10 cm sputter distance is optimal and can further enhance the charge mobility of electron-holes pairs within the plasma region. The presence of Ti-O-C bonds in the rGO-TiO$_2$ nanocomposite was determined using FTIR and XPS analyses. Besides, the DSSCs of the rGO-TiO$_2$ nanocomposite fabricated at a sputter distance of 10 cm possessed the highest PCE of 6.60%, suggesting that it is the ideal sputtering distance to achieve the fastest electron transfer and retarded charge recombination within the DSSCs' interfaces. The spontaneous increase of Voc to reach the maximum value of J_{sc} at the 10 cm sputter distance compared with the 5 cm sputter distance rGO-TiO$_2$ also demonstrated good light scattering and dye adsorption.

Acknowledgement

Table 3
Photovoltaic parameters of DSSCs fabricated with rGO-TiO$_2$ nanocomposites.

Sputtering distance (cm)	Short circuit current density, Jsc (mA cm^{-2})	Open circuit voltage, Voc (V)	Maximum point current, Imp (Amp)	Maximum point voltage, Vmp (V)	Fill factor, ff	Photovoltaic cell efficiency (PCE), η (%)
5	12.36	0.36	7.73	0.25	0.43	1.91
10	**15.82**	**0.72**	**11.40**	**0.58**	**0.58**	**6.60**
15	15.34	0.58	12.38	0.39	0.54	4.80
20	11.73	0.55	8.80	0.38	0.52	3.35
25	13.45	0.59	4.29	0.58	0.31	2.46

Appendix A. Supplementary material

Supplementary data to this article can be found online at https://doi.org/10.1016/j.solener.2019.05.069.

References

Achee, T.C., et al., 2018. High-yield scalable graphene nanosheet production from compressed graphite using electrochemical exfoliation. Sci. Rep. 8 (1), 14525.

Al-Rawashdeh, N.A., Albiss, B.A., Mo'ath, H., 2018. Graphene-based transparent electrodes for dye sensitized solar cells. IOP Conference Series: Materials Science and Engineering. IOP Publishing.

Al-Taweel, S.S., Saud, H.R., 2016. New route for synthesis of pure anatase TiO_2 nanoparticles via ultra sound assisted sol-gel method. J. Chem. Pharmaceut. Res. 8 (2), 620–626.

Berardi, U., 2017. A cross-country comparison of the building energy consumptions and their trends. Resour. Conserv. Recycl. 123, 230–241.

Chandra, K.A., Gill, S.S., 2017. Recent progress in dye sensitized solar cells. Int. J. Adv. Res., Ideas Innov. Technol. 3 (5), 77–85.

Chen, T., et al., 2012. Interface functionalization of photoelectrodes with graphene for high performance dye-sensitized solar cells. Adv. Funct. Mater. 22 (24), 5245–5250.

Chu, L., Qin, Z., Yang, J., 2015. Anatase TiO_2 nanoparticles with exposed 001 facets for efficient dye-sensitized solar cells. Sci. Rep. 5, 12143.

Ding, H., et al., 2015. Reduction of graphene oxide at room temperature with vitamin C for RGO–TiO_2 photoanodes in dye-sensitized solar cell. Thin Solid Films 584, 29–36.

Fujishima, A., Zhang, X., Tryk, D.A., 2008. TiO2 photocatalysis and related surface phenomena. Surf. Sci. Rep. 63 (12), 515–582.

Gao, J., et al., 2010. Environment-friendly method to produce graphene that employs vitamin C and amino acid. Chem. Mater. 22 (7), 2213–2218.

Gao, Y., et al., 2011. Reduced graphene oxide as a catalyst for hydrogenation of nitrobenzene at room temperature. Chem. Commun. 47 (8), 2432–2434.

Giordano, F., et al., 2016. Enhanced electronic properties in mesoporous TiO_2 via lithium doping for high-efficiency perovskite solar cells. Nat. Commun. 7, 10379.

Gómez-Navarro, C., et al., 2010. Atomic structure of reduced graphene oxide. Nano Lett. 10 (4), 1144–1148.

Hagfeldt, A., Vlachopoulos, N., 2018. Dye-sensitized solar cells. In: The Future of Semiconductor Oxides in Next-Generation Solar Cells. Elsevier, pp. 183–239.

Hamid, S.B.A., et al., 2014. Multiwalled carbon nanotube/TiO_2 nanocomposite as a highly active photocatalyst for photodegradation of Reactive Black 5 dye. Chin. J. Catal. 35(12).

How, G.T.S., et al., 2014. Highly exposed 001 facets of titanium dioxide modified with reduced graphene oxide for dopamine sensing. Sci. Rep. 4, 5044.

Jäger, T., et al., 2014. Controlling ion fluxes during reactive sputter-deposition of SnO_2: F. J. Appl. Phys. 116 (3), 033301.

Jiang, B., et al., 2011. In situ growth of TiO_2 in interlayers of expanded graphite for the fabrication of TiO_2–graphene with enhanced photocatalytic activity. Chem.–A Eur. J. 17 (30), 8379–8387.

Jin, Y.-S., et al., 2012. The effect of RF-sputtered TiO_2 passivating layer on the performance of dye sensitized solar cells. Ceram. Int. 38, S505–S509.

Kazmi, S.A., et al., 2017. Electrical and optical properties of graphene-TiO_2 nanocomposite and its applications in dye sensitized solar cells (DSSCS). J. Alloy. Compd. 691, 659–665.

Kim, S.R., Parvez, M.K., Chhowalla, M., 2009. UV-reduction of graphene oxide and its application as an interfacial layer to reduce the back-transport reactions in dye-sensitized solar cells. Chem. Phys. Lett. 483 (1–3), 124–127.

Lee, J.W., et al., 2012. A facile and template-free hydrothermal synthesis of Mn_3O_4 nanorods on graphene sheets for supercapacitor electrodes with long cycle stability. Chem. Mater. 24 (6), 1158–1164.

Li, W., et al., 2015. General strategy to synthesize uniform mesoporous TiO_2/graphene/mesoporous TiO_2 sandwich-like nanosheets for highly reversible lithium storage. Nano Letters 15 (3), 2186–2193.

Lim, S.P., et al., 2015. Reduced graphene oxide–titania nanocomposite-modified photoanode for efficient dye-sensitized solar cells. Int. J. Energy Res. 39 (6), 812–824.

Liu, Y., 2014. Hydrothermal synthesis of TiO 2–RGO composites and their improved photocatalytic activity in visible light. Rsc Advances 4 (68), 36040–36045.

Low, F.W., et al., 2018. Enhance of TiO_2 dopants incorporated reduced graphene oxide via RF magnetron sputtering for efficient dye-sensitised solar cells. Rare Met. 1–10.

Low, F.W., Lai, C.W., Hamid, S.B.A., 2015. Facile synthesis of high quality graphene oxide from graphite flakes using improved hummer's technique. Nanosci. Nanotechnol. 15, 1–5.

Low, F.W., Lai, C.W., Hamid, S.B.A., 2015. Easy preparation of ultrathin reduced graphene oxide sheets at a high stirring speed. Ceram. Int. 41 (4), 5798–5806.

Low, F.W., Lai, C.W., Hamid, S.B.A., 2017. Study of reduced graphene oxide film incorporated of TiO_2 species for efficient visible light driven dye-sensitized solar cell. J. Mater. Sci.: Mater. Electron. 28 (4), 3819–3836.

Low, F.W., Lai, C.W., Hamid, S.B.A., 2017. Surface modification of reduced graphene oxide film by Ti ion implantation technique for high dye-sensitized solar cells performance. Ceram. Int. 43 (1), 625–633.

Marcano, D.C., et al., 2010. Improved synthesis of graphene oxide. ACS Nano 4 (8), 4806–4814.

Naumenko, D., et al., 2012. Graphene-enhanced Raman imaging of TiO2 nanoparticles. Nanotechnology 23 (46), 465703.

Nouri, E., Mohammadi, M.R., Lianos, P., 2016. Impact of preparation method of TiO_2-RGO nanocomposite photoanodes on the performance of dye-sensitized solar cells. Electrochimica Acta 219, 38–48.

Novoselov, K.S., et al., 2004. Electric field effect in atomically thin carbon films. Science 306 (5696), 666–669.

Pan, L., et al., 2012. Morphology evolution of TiO_2 facets and vital influences on photocatalytic activity. ACS Appl. Mater. Interfaces 4 (3), 1650–1655.

Park, S., et al., 2011. Hydrazine-reduction of graphite-and graphene oxide. Carbon 49 (9), 3019–3023.

Pei, S., et al., 2010. Direct reduction of graphene oxide films into highly conductive and flexible graphene films by hydrohalic acids. Carbon 48 (15), 4466–4474.

Rambabu, Y., Jaiswal, M., Roy, S.C., 2016. Probing the charge recombination in rGO decorated mixed phase (anatase-rutile) TiO2 multi-leg nanotubes. AIP Adv. 6 (11), 115010.

Shang, Y., et al., 2015. Enhancing solar cell efficiency using photon upconversion materials. Nanomaterials 5 (4), 1782–1809.

Shen, J., et al., 2011. One step hydrothermal synthesis of TiO_2-reduced graphene oxide sheets. J. Mater. Chem. 21 (10), 3415–3421.

Sher Shah, M.S.A., et al., 2012. Green synthesis of biphasic TiO_2–reduced graphene oxide nanocomposites with highly enhanced photocatalytic activity. ACS Appl. Mater. Interfaces 4 (8), 3893–3901.

Song, J., et al., 2011. Enhancement of photogenerated electron transport in dye-sensitized solar cells with introduction of a reduced graphene oxide–TiO_2 junction. Chem.–A Eur. J. 17 (39), 10832–10837.

Song, C., et al., 2014. Dye-sensitized solar cells based on graphene-TiO_2 nanoparticles/TiO_2 nanotubes composite films. Int. J. Electrochem. Sci 9, 8090–8096.

Štengl, V., et al., 2013. TiO_2-graphene oxide nanocomposite as advanced photocatalytic materials. Chem. Cent. J. 7 (1), 41.

Tan, L.-L., et al., 2013. Reduced graphene oxide-TiO_2 nanocomposite as a promising visible-light-active photocatalyst for the conversion of carbon dioxide. Nanoscale Res. Lett. 8 (1), 465.

Tang, B., Hu, G., 2012. Two kinds of graphene-based composites for photoanode applying in dye-sensitized solar cell. J. Power Sources 220, 95–102.

Thakur, S., Karak, N., 2012. Green reduction of graphene oxide by aqueous phytoextracts. Carbon 50 (14), 5331–5339.

Wang, Z., et al., 2012b. Crystal facets controlled synthesis of graphene@ TiO_2 nanocomposites by a one-pot hydrothermal process. CrystEngComm 14 (5), 1687–1692.

Wang, W.-S., et al., 2012a. Large ultrathin anatase TiO_2 nanosheets with exposed 001 facets on graphene for enhanced visible light photocatalytic activity. J. Phys. Chem. C 116 (37), 19893–19901.

Wei, L., et al., 2018. Enhanced performance of the dye-sensitized solar cells by the introduction of graphene oxide into the TiO_2 photoanode. Inorg. Chem. Front. 5 (1), 54–62.

Williams, G., Seger, B., Kamat, P.V., 2008. TiO2-graphene nanocomposites. UV-assisted photocatalytic reduction of graphene oxide. ACS Nano 2 (7), 1487–1491.

Xiang, Q., Yu, J., Jaroniec, M., 2011. Enhanced photocatalytic H 2-production activity of graphene-modified titania nanosheets. Nanoscale 3 (9), 3670–3678.

Yan, W., et al., 2014. A novel 3D structured reduced graphene oxide/TiO_2 composite: synthesis and photocatalytic performance. J. Mater. Chem. A 2 (10), 3605–3612.

Yen, C.-C., et al., 2011. Improving conversion efficiency of dye-sensitized solar cells by metal plasma ion implantation of ruthenium ions. Thin Solid Films 519 (15), 4717–4720.

Yu, R., Pruneri, V., De Abajo, F.J.G., 2016. Active modulation of visible light with graphene-loaded ultrathin metal plasmonic antennas. Sci. Rep. 6, 32144.

Zhang, H., et al., 2011. A facile one-step synthesis of TiO 2/graphene composites for photodegradation of methyl orange. Nano Res. 4 (3), 274–283.

Zhang, Y., et al., 2017. Reduced graphene oxide wrapped mesoporous hierarchical TiO_2-CdS as a photoanode for high-performance dye-sensitized solar cells. Eur. J. Inorg. Chem. 2017 (16), 2281–2288.

Zhou, K., et al., 2011. Preparation of graphene–TiO_2 composites with enhanced photocatalytic activity. New J. Chem. 35 (2), 353–359.